The Journal of Immunology

RESEARCH ARTICLE | APRIL 15 2015

Deficiency of MALT1 Paracaspase Activity Results in Unbalanced Regulatory and Effector T and B Cell Responses Leading to Multiorgan Inflammation

Frédéric Bornancin; ... et. al

J Immunol (2015) 194 (8): 3723–3734.
https://doi.org/10.4049/jimmunol.1402254

Deficiency of MALT1 Paracaspase Activity Results in Unbalanced Regulatory and Effector T and B Cell Responses Leading to Multiorgan Inflammation

Frédéric Bornancin,*[,1] Florian Renner,*[,1] Ratiba Touil,* Heiko Sic,* Yeter Kolb,* Ismahane Touil-Allaoui,* James S. Rush,* Paul A. Smith,* Marc Bigaud,* Ursula Junker-Walker,* Christoph Burkhart,* Janet Dawson,* Satoru Niwa,* Andreas Katopodis,* Barbara Nuesslein-Hildesheim,* Gisbert Weckbecker,* Gerhard Zenke,* Bernd Kinzel,* Elisabetta Traggiai,* Dirk Brenner,[†,‡] Anne Brüstle,[†,§] Michael St. Paul,[†] Natasa Zamurovic,* Kathy D. McCoy,[¶] Antonius Rolink,[‖] Catherine H. Régnier,* Tak W. Mak,[†] Pamela S. Ohashi,[†] Dhavalkumar D. Patel,* and Thomas Calzascia*

The paracaspase MALT1 plays an important role in immune receptor-driven signaling pathways leading to NF-κB activation. MALT1 promotes signaling by acting as a scaffold, recruiting downstream signaling proteins, as well as by proteolytic cleavage of multiple substrates. However, the relative contributions of these two different activities to T and B cell function are not well understood. To investigate how MALT1 proteolytic activity contributes to overall immune cell regulation, we generated MALT1 protease-deficient mice (*Malt1*$^{PD/PD}$) and compared their phenotype with that of MALT1 knockout animals (*Malt1*$^{-/-}$). *Malt1*$^{PD/PD}$ mice displayed defects in multiple cell types including marginal zone B cells, B1 B cells, IL-10–producing B cells, regulatory T cells, and mature T and B cells. In general, immune defects were more pronounced in *Malt1*$^{-/-}$ animals. Both mouse lines showed abrogated B cell responses upon immunization with T-dependent and T-independent Ags. In vitro, inactivation of MALT1 protease activity caused reduced stimulation-induced T cell proliferation, impaired IL-2 and TNF-α production, as well as defective Th17 differentiation. Consequently, *Malt1*$^{PD/PD}$ mice were protected in a Th17-dependent experimental autoimmune encephalomyelitis model. Surprisingly, *Malt1*$^{PD/PD}$ animals developed a multiorgan inflammatory pathology, characterized by Th1 and Th2/0 responses and enhanced IgG1 and IgE levels, which was delayed by wild-type regulatory T cell reconstitution. We therefore propose that the pathology characterizing *Malt1*$^{PD/PD}$ animals arises from an immune imbalance featuring pathogenic Th1- and Th2/0-skewed effector responses and reduced immunosuppressive compartments. These data uncover a previously unappreciated key function of MALT1 protease activity in immune homeostasis and underline its relevance in human health and disease. ***The Journal of Immunology*****, 2015, 194: 3723–3734.**

Uncontrolled NF-κB activation can lead to lymphoproliferative disorders and autoimmune diseases associated with chronic inflammation, underscoring the need for appropriate regulation of signaling via this commonly used pathway (1–4). The paracaspase MALT1 plays an important role in the regulation of NF-κB (5). Upon activation by Ag receptors, Dectin receptors, or G protein–coupled receptors, MALT1 and the caspase recruitment domain (CARD)–containing protein BCL10 assemble with another CARD-containing protein: CARD11 (also known as CARMA-1), CARD9, or CARD10, respectively. The resulting CARD-BCL10-MALT1 (CBM) complex functions as a hub for triggering a signaling cascade that culminates in activation of the IκB kinase (IKK) complex, IκB degradation, and NF-κB activation (6, 7).

MALT1 regulates NF-κB activity in at least two ways. First, its scaffolding function is essential for NF-κB activation (8, 9).

*Novartis Institutes for BioMedical Research, Novartis Pharma AG, 4056 Basel, Switzerland; [†]Campbell Family Institute for Breast Cancer Research, Princess Margaret Cancer Centre, University Health Network, Toronto, Ontario M5G 2C1, Canada; [‡]Department of Infection and Immunity, Luxembourg Institute of Health, L-4354 Esch-Sur-Alzette, Luxembourg; [§]Department of Immunology, John Curtin School of Medical Research, The Australian National University, Canberra ACT 2601, Australia; [¶]Maurice Müller Laboratories, University Clinic for Visceral Surgery and Medicine, University of Bern, 3010 Bern, Switzerland; and [‖]Developmental and Molecular Immunology, Department of Biomedicine, University of Basel, 4058 Basel, Switzerland

[1]F.B. and F.R. are co-first authors.

Received for publication September 3, 2014. Accepted for publication February 7, 2015.

This work was supported by a Presidential Postdoctoral Fellowship from Novartis Institutes for BioMedical Research (to F.R. and H.S.) and the ATTRACT program of the Luxembourg National Research Fund (to D.B.).

Address correspondence and reprint requests to Dr. Thomas Calzascia, Novartis Institutes for BioMedical Research, Novartis Pharma AG, WSJ-386, Kohlenstrasse, CH-4056 Basel, Switzerland. E-mail address: thomas.calzascia@novartis.com

The online version of this article contains supplemental material.

Abbreviations used in this article: BM, bone marrow; CARD, caspase recruitment domain; CBM, CARD-BCL10-MALT1 complex; cerLN, cervical and mandibular LN; CYLD, cylindromatosis; DAGG, 2,4-dinitrophenyl-β-alanyl-glycyl-glycyl-*N*(2-aminoethyl)carbamyl-methylated; EAE, experimental autoimmune encephalomyelitis; FO, follicular; GC, germinal center; IKK, IκB kinase; KLH, keyhole limpet hemocyanin; LN, lymph node; mesLN, mesenteric LN; MOG, myelin oligodendrocyte glycoprotein; MZ, marginal zone; PD, protease dead; PEL, peritoneal exudate cells; PP, Peyer's patches; T_{CM}, central memory T; TD, T-dependent; T_{EM}, effector memory T; T_{FH}, follicular Th; TI, T-independent; TI-2, T-independent type 2; Treg, regulatory T cell; WT, wild-type.

www.jimmunol.org/cgi/doi/10.4049/jimmunol.1402254

Second, MALT1 has proteolytic activity targeting several substrates important in NF-κB signaling (10). These include BCL10, whose cleavage by MALT1 appears to regulate integrin-dependent T cell adhesion (11). The other known substrates of MALT1 are all negative regulators of canonical NF-κB signaling. MALT1-dependent cleavage of the two ubiquitin editing enzymes, A20 and cylindromatosis (CYLD), downregulates their activity (12–15). MALT1 also cleaves RelB, priming it for proteasome-dependent degradation (16) and resulting in modulation of canonical NF-κB activation via the release of RelA and c-Rel. In addition, Regnase-1, an RNase that destabilizes a subset of NF-κB–dependent mRNAs by cleaving their 3′ termini (e.g., c-Rel and IL-2), is also proteolyzed and inactivated by MALT1 (17). Thus, MALT1 regulates the NF-κB cascade by acting as a scaffolding partner within the CBM complex enabling signaling, and as a protease by cleaving key regulatory proteins, thereby sustaining NF-κB activation.

Previous reports using MALT1, CARD11-, and BCL10-deficient cells have established that the CBM complex is essential for NF-κB signaling in T and B cells (8, 9, 18–20). However, the relevance of MALT1 protease versus scaffolding activities in relation to immune function and the long-term consequences associated with the abrogation of MALT1 enzymatic activity in vivo are still unclear. To investigate this point, we generated and characterized a novel MALT1 protease dead (PD) mouse line ($Malt1^{PD/PD}$). In this study, we describe an unexpected phenotype of $Malt1^{PD/PD}$ mice, as well as the impact of constitutive disruption of MALT1 enzymatic activity on lymphocyte compartments and general immune homeostasis. A direct comparison with MALT1 knockout ($Malt1^{-/-}$) mice enabled us to delineate the respective contributions of scaffolding and proteolytic functions of MALT1 in the regulation of T and B cell–mediated immunity.

Materials and Methods

Generation of $Malt1^{PD/PD}$ *and* $Malt1^{-/-}$ *mice and genotyping*

To generate a targeting vector for homologous recombination, we amplified MALT1 genomic sequences from C57BL/6 mouse genomic DNA. First, a 1.6-kb DNA fragment containing *Malt1* exons 10 and 11 was amplified by PCR, and a cysteine-to-alanine mutation was introduced at aa position 472 by overlapping PCR. The mutated fragment was cloned into vector pRAY 2loxP 2FRT in between the two loxP sites. Next, a 2.5-kb genomic fragment corresponding to *Malt1* intron 9 was amplified and cloned in front of the 5′ loxP site. Finally, 1.7-kb *Malt1* genomic DNA downstream of exon 11 was amplified and subcloned behind the FRT flanked neomycin cassette of pRAY 2loxP 2FRT, resulting in the final *Malt1* targeting construct for homologous recombination. Subcloned sequences were compared with sequences available from the Ensembl database (Ensembl Gene ID ENSMUSG00000032688).

After introduction into C57BL/6 embryonic stem cells, neomycin-resistant clones were screened by PCR for homologous recombination. Correct targeting was confirmed by Southern blot using a neomycin-specific probe that allowed the exclusion of random integration events of the targeting vector. Selected targeted embryonic stem cells were injected into BALB/c blastocysts and chimeric mice were bred with C57BL/6 females, resulting in an F1 generation of heterozygous MALT1 gene–targeted mice ($Malt1^{PD/WT}$). To eliminate the FRT-flanked neomycin cassette, we crossed $Malt1^{PD/WT}$ mice with a mouse line expressing Flp recombinase. Homozygous $Malt1^{PD/PD}$ mice were generated by the interbreeding of $Malt1^{PD/WT}$ animals.

To generate $Malt1^{-/-}$ animals, we bred $Malt1^{PD/WT}$ mice with a Cre5 mouse line to excise exons 10 and 11 of the *Malt1* gene (Supplemental Fig. 1A). Successive breeding was used to generate homozygous $Malt1^{-/-}$ animals devoid of the Cre recombinase gene. Genotyping was performed using the following primer sets: Forward 5′-CCAGCCATGTGACTTGAAGC-3′, and Reverse: 5′-GGGCTATTGAGGTAGGGTC-3′, 5′-ACACGGACGGATATGCTAGGCA-3′.

Generation of bone narrow chimeras

To generate bone marrow (BM) chimeras, we injected 10^6 BM cells derived from female CD45.2 wild-type (WT), $Malt1^{PD/PD}$, or $Malt1^{-/-}$ mice i.v. into 10-wk-old sublethally irradiated (2 times 450 rad 4 h apart) CD45.1 female WT recipients (B6.SJL-Ptprc^{a}Pepc^b/BoyJ; Taconic). BM cells were isolated by flushing femur and tibiae using RPMI 1640 media and subsequently depleted of RBC by hypotonic shock using ACK buffer: 0.829% NH_4Cl, 0.1% $KHCO_3$, and 0.0372% EDTA.

*DNP-keyhole limpet hemocyanin and 2,4-dinitrophenyl-β-alanyl-glycyl-glycyl-*N*(2-aminoethyl)carbamyl-methylated–Ficoll immunization and titer measurement*

Keyhole limpet hemocyanin (KLH; Calbiochem) conjugated to DNP (Sigma-Aldrich) was prepared, at a ratio of 1/20, as DNP-KLH stock solution (5 mg/ml) and stored at −20°C. DAGG (2,4-DNP-β-alanyl-glycyl-glycyl-N(2-aminoethyl)carbamyl-methylated)–Ficoll conjugate was prepared as described previously (21).

For induction of T-dependent (TD) responses, DNP-KLH was adsorbed onto colloidal aluminum hydroxide (Alu-Gel-S, SERVA: 1 ml DNP-KLH/5 ml Alu-Gel-S/4 ml PBS) and injected i.p. into mice at 100 μg/0.2 ml/mouse. For induction of T-independent (TI) type 2 (TI-2) responses, DAGG-Ficoll was injected in PBS i.v. into mice at 20 μg/0.2 ml/mouse. DNP-specific IgG and IgM levels were measured in serum on days 8 (DNP-KLH) or 6 (DAGG-Ficoll) postimmunization. Ab titers were measured by ELISA and are expressed as mean ± SEM log10 dilution values using 50% of the maximal extinction at 405 nm as the end point.

T cell activation, proliferation, and differentiation

For T cell proliferation assays, total $CD3^+$ T cells purified from spleens using the CD3 isolation kit (Miltenyi Biotec) were cultured in IMDM (Life Technologies), 10% FCS (Amimed), 50 μM 2-ME (Life Technologies), and 100 U/ml penicillin/streptomycin. Purified T cells (10^5/well) were plated on flat-bottom 96-well plates coated overnight with the indicated concentrations of anti-CD3 Ab (clone 145-2C11; BD Biosciences) and anti-CD28 Ab (clone 37-51; BD Biosciences). Three days after stimulation, plates were pulsed with 1 μCi/well [^{3}H]thymidine (Amersham) for 5 h and incorporation of [^{3}H]thymidine was measured using a β-plate counter (Wallac).

Ex vivo T cell stimulation for cytokine release or intracellular cytokine staining was performed on total LN or spleen cells. In brief, 2.5×10^6 cells/ml were stimulated for 4 h at 37°C in 24-well plates in the presence of 100 ng/ml PMA (Sigma-Aldrich) and 100 ng/ml ionomycin (Sigma-Aldrich). For cytokine secretion assays, supernatants were collected 4 h after stimulation and cytokine levels were analyzed using Meso Scale Discovery following the manufacturer's instructions and an MSD Sector Imager 6000. Cell stimulation for intracellular cytokine staining was performed in the presence 1 μl/ml GolgiStop (BD Biosciences).

For in vitro Th cell differentiation assays, naive $CD4^+CD62L^+$ Th cells were isolated from spleens and LN, and sorted using a magnetic bead cell purification kit according to the manufacturer's instructions (Miltenyi Biotec). For priming, enriched Th cells were stimulated for 96 h with 1 μg/ml plate-bound anti-CD3 Ab plus 1–2 μg/ml anti-CD28 Ab (BD Biosciences). Naive cells were induced to differentiate into regulatory T cells (Tregs) by addition of 3 ng/ml recombinant human TGF-β (rhTGF-β; R&D), 50 U/ml rhIL-2 (Peprotech), and 5 μg/ml anti–IFN-γ Ab (BD Biosciences), and into Th1 cells by addition of 4 ng/ml IL-12 (Peprotech) plus 50 U/ml rhIL-2. For differentiation of Th17 cells, naive Th cells received 5 μg/ml anti–IFN-γ Ab, 30 ng/ml rmIL-6 (Peprotech), 2 ng/ml rhTGF-β, and 50 U/ml rhIL-2.

FACS analysis and reagents

FACS stainings of cell suspensions from spleen, LN, and Peyer's patches (PP) were prepared by passing tissues through a 70-μm sieve followed by RBC lysis using ACK buffer. Cells were washed once in FACS buffer (PBS containing 2% FCS, 0.05% NaN_3), blocked with mouse Fc Block (BD Biosciences), and stained for 30 min at 4°C with the indicated combination of fluorochrome-conjugated Abs. After staining, the cells were washed twice and resuspended in 200 μl buffer before acquisition on a FACSCantoII or FACSFortessa flow cytometer. Data were analyzed using the FlowJo software.

The Abs used were obtained from different sources: B220, CD25, CD3, CD4, CD8, CD11b, CD45.1, CD45.2, Foxp3, GL7, IgD, IgM, PD1, TNF-α, and streptavidin from eBioscience; CD4, CD11c, CD19, CD44, CXCR5, IFN-γ, IL-2, IL-17a, and TNF-α from BD Biosciences; CD3, CD5, CD8, CD21/CD35, CD23, CD62L, and IgG1 from Biolegend; peanut agglutinin–FITC from Vector Laboratory.

Histology, immunofluorescence, and serum Ig measurements

Histological analyses were performed on formalin-fixed organs using standard protocols and Ig levels assessed by the Luminex technology.

Immunofluorescence stainings were performed on OCT-embedded snap-frozen tissues.

At necropsy, a series of organs/tissues were sampled, fixed in neutral phosphate-buffered formalin, embedded in paraffin wax, sectioned, and stained with H&E. Bone was demineralized with formic acid. The histological slides were examined by light microscopy. Lymphoid cell infiltrates were characterized by immunohistochemistry for T cells (CD3) and B cells (B220).

For immunofluorescence stainings, spleens and mesenteric LN (mesLN) were snap frozen, OCT-embedded, and 5-μm cryosections were prepared. Sections were fixed in acetone for 10 min and then air-dried for 60 min. Spleen sections were stained with anti–IgM-FITC, anti–IgD-Alexa 647, and Moma-PE. mesLN sections were stained with anti–IgM-FITC, anti–IgD-Alexa 647, and peanut agglutinin–PE.

Serum and intestinal lavage Ig concentrations were determined by the Luminex xMAP technology using the IgE Single Plex Magnetic Bead Kit and the Ig Isotyping Magnetic Bead Panel (Merck Millipore) with a Luminex 200 instrument according to manufacturer's instructions.

Treg adoptive transfer

For Treg reconstitution experiments, transferred cells were FACS sorted from LN and spleen cells collected from EGFP-Foxp3 knock-in mice (Jackson Laboratory). In brief, pooled LN and spleens were stained with fluorescently labeled CD4 Ab and $EGFP^+CD4^+$ (i.e., $Foxp3^+$), and $EGFP^{neg}$ $CD4^+$ (i.e., $Foxp3^{neg}$) cell populations were sorted using a FACSAria. Freshly sorted cells were then injected i.v. (5×10^5 cells/mouse) into 8- to 9-wk-old female *Malt1*$^{PD/PD}$ mice. Mice were subsequently monitored for weight loss and signs of pathology development.

B cell activation

B cell proliferation assays were performed on total splenic B cells purified by negative selection using an EasySep Mouse B Cell Enrichment Kit (Stemcell Technologies). Cells were plated at 10^5 cells/well on flat-bottom 96-well plates in RPMI 1640, 1 mM sodium pyruvate, nonessential amino acids, 50 μM 2-ME, 100 U/ml penicillin and 100 μg/ml streptomycin (Life Technologies), and 10% FCS (Amimed). Cells were stimulated with 10 μg/ml CpG1826 (Invivogen), 25% of the CD40L-containing supernatant from cell line 8-40-19 with or without 125 U/ml IL-4 (derived from CHO-mouse IL-4 KI-5; Novartis), 50 ng/ml LPS from *Salmonella enterica* (Sigma-Aldrich) or 25 μg/ml anti-IgM Ab (Jackson Immunoresearch) supplemented with 5 ng/ml IL-4 (Peprotech). On day 3 of culture, cells were pulsed with 1 μCi/well [^{3}H]thymidine (Amersham), and 5 h later incorporation of [^{3}H]thymidine was measured using a β-plate counter (Wallac).

For experiments assessing TLR-ligand–induced cytokine release, cells were stimulated overnight with ssRNA40 (200 μg/ml) and CpG1826 (20 μM) (Invivogen). Levels of TNF-α, IL-6, and IL-10 in culture supernatants were measured using Meso Scale Discovery.

Immunoblotting

$CD3^+$ T cells were isolated from pooled LN using the mouse T cell enrichment kit (Stemcell Technologies). $CD19^+$ B cells were isolated from pooled spleens using the mouse B cell enrichment kit (Stemcell Technologies). A total of 1.4×10^7 purified $CD3^+$ T cells or $CD19^+$ B cells were stimulated for the indicated times using 40 ng/ml PMA and 1 μM Ionomycin. Cells were collected by centrifugation and resuspended in lysis buffer (36 μM β-glycerophosphate pH 7.5, 1% Nonidet P-40, 0.5% Na cholate, 0.1% SDS, 2 mM DTT, 1% phosphatase inhibitor mixture 2 and 3 [Sigma-Aldrich] supplemented with complete protease inhibitor mixture [Roche]). After 5-min incubation on ice, cell lysates were cleared by centrifugation at 13,000 × *g* for 10 min. Proteins were separated on 4–12% Bis-Tris SDS-PAGE gradient gels (Life Technologies) and transferred to polyvinylidene difluoride membranes (Life Technologies), and immunoblots were incubated with the indicated Abs. Finally, proteins were detected by fluorescence using an Odyssey imager following the instructions given by the manufacturer (Li-COR Biosciences).

Abs used for Western blot detection were anti-MALT1 (H-300) and anti-CYLD (E-10) from Santa Cruz Biotechnology; anti-RelB (C1E4), anti-IκBα, anti–phospho-IκBα (Ser32) (5A5), anti–stress-activated protein kinase/JNK, anti-phospho–stress-activated protein kinase /JNK (Thr^{183}/Tyr^{185}) (G9), anti–phospho-p44/42 MAPK (Erk1/2) (Thr^{202}/Tyr^{204}) (D13.14.4E) from Cell Signaling Technology; anti-Regnase (MCPIP1) (604421) from R&D, and anti–α-tubulin (tub 2.1) from Sigma-Aldrich. IRDye 800CW goat anti-rabbit (H+L) and Alexa Fluor 680 $F(ab')_2$ fragment of goat anti-mouse IgG (H+L) secondary Abs were from Li-COR Biosciences and Life Technologies, respectively.

Quantitative PCR analysis

Splenic CD4 T cells were isolated by MACS separation (Miltenyi Biotec) and activated with PMA (100 ng/ml) and Ionomycin (100 ng/ml). At the indicated time points, RNA was extracted with the RNeasy Plus Mini Kit (Qiagen) and reverse transcription of equivalent amounts of RNA was performed using the QuantiTect Reverse Transcription Kit (Qiagen). For quantitative PCR, cDNA fragments were amplified through the use of TaqMan Fast Universal PCR Master Mix and TaqMan probes for mouse c-Rel and IL-2 (Applied Biosystems). Fluorescence was detected with a 7500 fast real-time PCR system (Applied Biosystems). The mRNA expression level was normalized to the expression level of β_2-microglobulin, and changes were calculated using the ΔΔ cycle threshold method.

Experimental autoimmune encephalomyelitis induction

Nine-week-old male WT or *Malt1*$^{PD/PD}$ mice (n = 10/group) were s.c. immunized at the lower back with myelin oligodendrocyte glycoprotein (MOG_{1-125}, in-house produced; 200 μg/100 μl) emulsified in 4 mg/ml CFA (Sigma-Aldrich). Pertussis toxin (Fluka; 200 ng/mouse) was administered i.p. on days 0 and 2. Experimental autoimmune encephalomyelitis (EAE) development was monitored daily using the well-established scoring system (0, normal appearance; 1, complete tail paralysis; 2, unilateral partial hind-limb paralysis; 3, complete bilateral hind-limb paralysis; 4, quadriplegia; 5, death).

Statistics

Bar graphs in the figures represent average values ± SEM unless indicated otherwise. Statistical significance between groups was calculated using a two-tailed unpaired Student t test or a Kruskal–Wallis one way ANOVA using GraphPad Prism (GraphPad Software) and is indicated in the graphs as follows: $*p < 0.05$, $**p < 0.01$, $***p < 0.001$. Nonsignificant differences were not indicated.

Study approval

Procedures involving animals were carried out on Experimental Animal Licenses approved by the regional governmental authorities. All efforts were made to minimize animal suffering, and *Malt1*$^{PD/PD}$ mice were humanely killed before or as soon as the first signs of pathology were noticed.

Results

Malt1$^{PD/PD}$ *mice express catalytically inactive MALT1 and display normal activation of the IKK, JNK, and ERK pathways in T and B lymphocytes*

To study the physiological relevance of MALT1 enzymatic function, we generated and characterized a novel PD MALT1 knock-in mouse line (*Malt1*$^{PD/PD}$) where the protease function of MALT1 was specifically ablated by mutating the active site cysteine (C472A). Because of the specific design of the targeting vector, it was possible to generate a control *Malt1*$^{-/-}$ mouse line that originated from the same targeted offspring as the *Malt1*$^{PD/PD}$ mice (Supplemental Fig. 1A). *Malt1*$^{PD/PD}$ and *Malt1*$^{-/-}$ mice were born at rates close to the expected Mendelian ratio (Supplemental Fig. 1B) and displayed a normal growth and behavior until at least 8–9 wk of age.

To confirm the impact of the alterations in the *Malt1* gene introduced by the targeting strategy on the expression and function of MALT1 protein, we assessed purified splenic T and B cells from the different mouse strains for MALT1 protein levels and function, as well as for PMA/ionomycin-induced activation of NF-κB, ERK, and JNK pathways. As expected, MALT1 protein was undetectable in *Malt1*$^{-/-}$ lymphocytes, whereas the C472A MALT1 mutant was expressed in *Malt1*$^{PD/PD}$ lymphocytes to a similar level as in WT cells (Fig. 1A and 1B). Cleavage of CYLD, a reported MALT1 substrate important for the regulation of JNK, was abrogated in *Malt1*$^{PD/PD}$ T cells, confirming that the C472A mutation rendered MALT1 catalytically inactive. Consistently, cleavage of two further MALT1 substrates, RelB and Regnase-1, was also fully blocked in *Malt1*$^{PD/PD}$ T cells (Fig. 1A).

Phosphorylation of the IKK substrate IκBα was clearly detectable in *Malt1*$^{PD/PD}$ T cells but blocked in the absence of

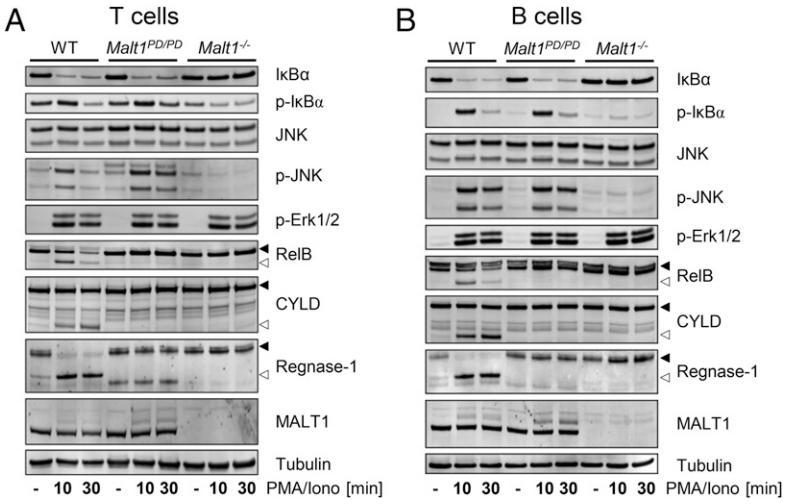

FIGURE 1. Biochemical characterization of *Malt1*$^{PD/PD}$ and *Malt1*$^{-/-}$ T and B lymphocytes. Immunoblot analysis of purified splenic T cells (**A**) or B cells (**B**) from WT, *Malt1*$^{PD/PD}$, and *Malt1*$^{-/-}$ mice stimulated with PMA/ionomycin (PMA/Iono) for the indicated times. Immunoblotting for tubulin served as a loading control. Black and open arrowheads indicate uncleaved and cleaved MALT1 substrates, respectively. Cells of seven (A) or five mice (B) per genotype were pooled. Data are representative of at least two independent experiments.

MALT1 protein (Fig. 1A), indicating that IKK activity is largely independent of MALT1 proteolytic function. Consistent data were obtained with other IKK substrates such as p65 and p105 (data not shown). Similarly, normal phosphorylation of JNK and ERK kinases in *Malt1*$^{PD/PD}$ T cells indicated independency of these pathways from MALT1 proteolytic function. These results show that the proteolytic function of MALT1 is not essential for acute IKK, JNK, and ERK signaling. Furthermore, they suggest that catalytically inactive MALT1 is able to scaffold properly. Supporting this, PMA/ionomycin stimulation induced high m.w. MALT1 species (Fig. 1A) consistent with monoubiquitinated MALT1, a recently identified modification of MALT1 that results from scaffold-induced MALT1 processing by a mechanism that remains to be elucidated (22).

Similarly to the observations in T lymphocytes, PMA/ionomycin-stimulated purified B cells displayed normal acute phosphorylation of IκBα and JNK in the absence of MALT1 proteolytic function, whereas the same process was suppressed in the absence of MALT1 protein (Fig. 1B). Phosphorylation of ERK was also confirmed to occur independently of MALT1 as both *Malt1*$^{PD/PD}$ and *Malt1*$^{-/-}$ B cells displayed normal ERK phosphorylation in response to PMA/ionomycin (Fig. 1B). As observed in T cells, increased levels of putative monoubiquitinated MALT1 species were observed upon stimulation of *Malt1*$^{PD/PD}$ B cells, supporting an intact scaffolding ability of catalytically inactive MALT1. Cleavage of RelB, Regnase-1, and CYLD was also abolished in *Malt1*$^{PD/PD}$ B cells (Fig. 1B).

Collectively, these biochemical data provide evidence for normal expression of the catalytically inactive MALT1 C472A mutant protein in *Malt1*$^{PD/PD}$ mice and show that activation-induced IKK, ERK, and JNK activation can occur independently of the proteolytic function of MALT1.

Malt1$^{PD/PD}$ *mice develop a spontaneous multiorgan inflammatory pathology*

Similarly to other *Malt1*$^{-/-}$ mouse lines (8, 9), the *Malt1*$^{-/-}$ mice described in this article were viable and displayed normal behavior and life span. Unexpectedly, at the age of 9–10 wk, *Malt1*$^{PD/PD}$ animals started developing pathological symptoms, including weakness, hunched posture, eye inflammation, and hindlimb paralysis, ultimately leading to weight loss and death. The incidence of the pathology was more apparent in female *Malt1*$^{PD/PD}$ mice (Supplemental Fig. 1C). Extensive macroscopic and histopathology analyses, performed on 8- to 12-wk-old *Malt1*$^{PD/PD}$ mice, revealed minimal-to-moderate lymphoid cell infiltration in a variety of organs, mainly glandular stomach, lacrimal, salivary, and Harderian glands, lungs, and peripheral nerves (Fig. 2A–L, Supplemental Fig. 2, and data not shown). Affected nerves included the sciatic and spinal nerves, as well as small peripheral nerve fibers such as the pharyngeal nerve (Supplemental Fig. 2 and data not shown). No alterations were observed in brain, spinal cord, or optic nerve (data not shown). Minimal-to-moderate lymphoid hyperplasia and plasma cell hyperplasia were evident in lymph nodes (LN), particularly mandibular LN and mesLN (Fig. 2F). Lymphoid hyperplasia was also present in the GALT of the small intestine (data not shown). A predominance of B cells over T cells was observed in the glandular stomach, salivary and lacrimal glands, and the GALT. Lymphoid infiltrates in the lungs, the Harderian glands, and the small nerve fibers consisted mainly of T cells. Ex vivo analysis of thymus, spleen, pooled cervical and mandibular LN (cerLN), mesLN, inguinal LN, PP, and peritoneal exudate cells (PEL) confirmed the increased cellularity of mesLN, cerLN, and PP in *Malt1*$^{PD/PD}$ mice and revealed normal splenic, thymic, and inguinal LN size (Fig. 2M). *Malt1*$^{-/-}$ mice also exhibited a significant increase in mesLN and cerLN cellularity, but the extent was less pronounced when compared with *Malt1*$^{PD/PD}$ mice.

Analysis of serum Ig levels in *Malt1*$^{-/-}$ mice confirmed the previously reported reduction in serum IgM and IgG, and revealed reduced IgE levels (Fig. 2N) (8, 9). *Malt1*$^{PD/PD}$ mice had reduced IgM, IgG2a, IgG2b, and IgG3 levels, but in contrast displayed a significant elevation in both serum IgG1 and IgE. Serum and intestinal IgA levels were not altered in *Malt1*$^{PD/PD}$ mice.

Thus, the selective abrogation of the proteolytic function of MALT1 resulted in a progressive inflammatory pathology associated with partial lymphadenopathy, multiorgan infiltration by T and B cells, and increased IgG1 and IgE levels.

Malt1$^{PD/PD}$ *mice display partial impairment of the B cell compartment and follicular T cells and abrogated B cell responses to active Ag immunization*

Given the high prevalence of B cells in affected tissues of *Malt1*$^{PD/PD}$ mice and the increased IgG1 and IgE levels, we characterized in more detail the composition and function of the B cell compartment in these mice.

In line with previous reports, *Malt1*$^{-/-}$ mice displayed a normal development of splenic follicular (FO) B cells and a severe reduction of marginal zone (MZ) B cells and peritoneal B1 B cells (8, 9) (Fig. 3A and 3B). Similarly, peritoneal B1 B cells were absent in *Malt1*$^{PD/PD}$ mice, indicating that proteolytic function of

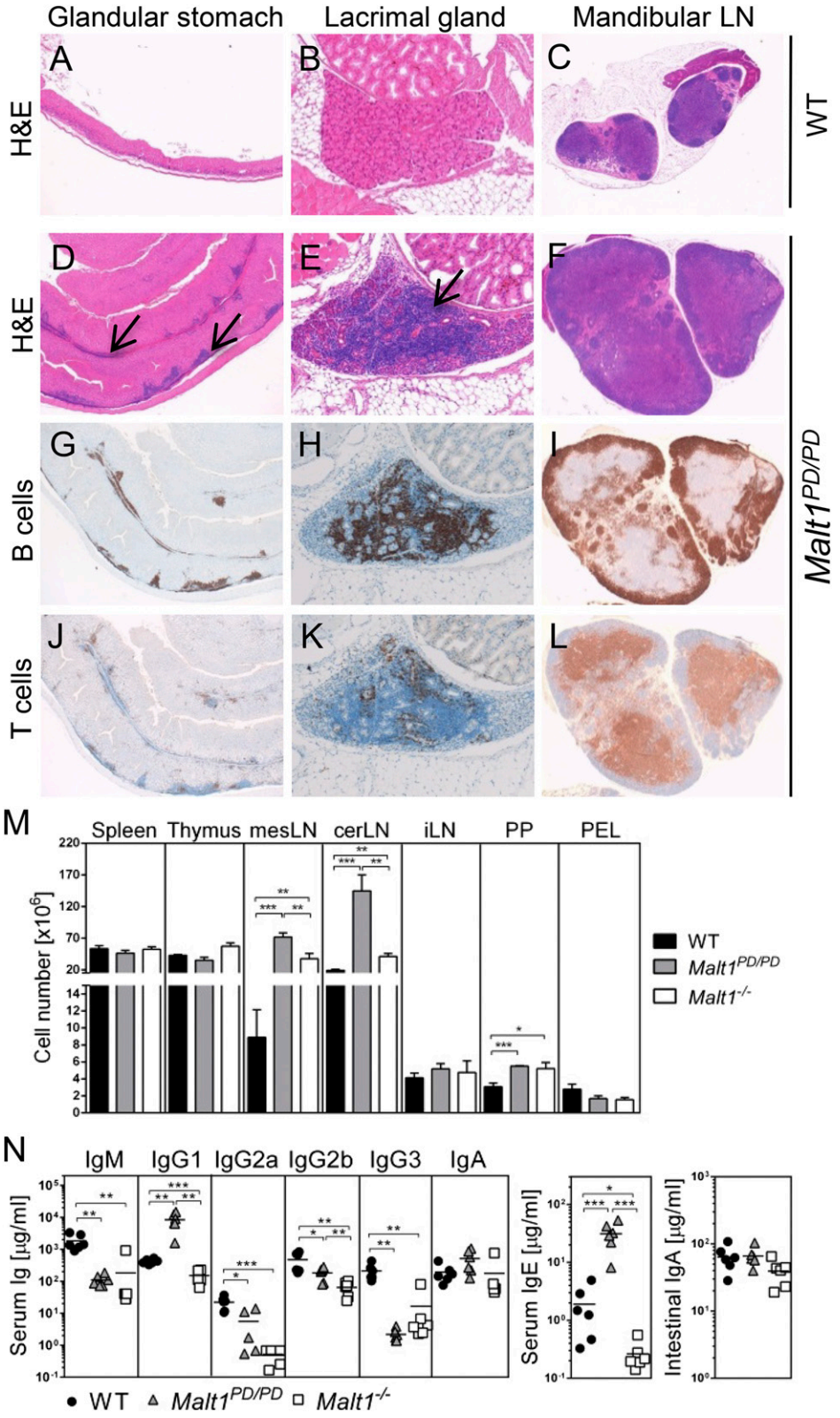

FIGURE 2. Histological alterations and serum Ig levels in *Malt1*$^{PD/PD}$ mice. (**A**–**F**) H&E staining of different tissues from WT (A–C) and *Malt1*$^{PD/PD}$ mice (D–F). (D–F) Moderate lymphoid cell infiltration (arrows) in glandular stomach (D), lacrimal gland (E), and lymphoid hyperplasia of mandibular LN (F) of *Malt1*$^{PD/PD}$ mice. (**G**–**L**) Immunohistochemical staining for B220 (G–I) and CD3 (J–L). Original magnification ×2 (A, C, D, F, G, I, J, and L), ×10 (B, E, H, and K). (**M**) Cellularity of the major lymphoid organs and PEL. Bars represent mean ± SEM (n = 5 mice/group). Data are representative of three independent experiments. (**N**) Serum Ig and intestinal IgA levels (n = 6 per group). Serum Ig data are representative of at least three independent experiments. Statistical significance was calculated using a two-tailed unpaired t test (*p < 0.05, **p < 0.01, ***p < 0.001).

MALT1 was essential for the development and/or survival of this innate B cell population. Although splenic FO B cells were not affected, a reduced, but detectable MZ B cell population was present in *Malt1*$^{PD/PD}$ mice (Fig. 3B, Supplemental Fig. 3A and 3B).

Further characterization of germinal center (GC) B cells revealed an almost complete absence of GC B cells in all lymphoid organs of *Malt1*$^{-/-}$ mice, including PP and mesLN (Fig. 3C, Supplemental Fig. 3C and 3D, and data not shown). The absence of GC B cells correlated with a severe reduction in CD4$^+$CXCR5$^+$PD1$^+$ follicular Th (T_{FH}) cells (Fig. 3D). By contrast, *Malt1*$^{PD/PD}$ mice retained normal or partially reduced proportions of GC B cells in PP, mesLN, and cerLN (Fig. 3C, Supplemental Fig. 3C and 3D). In line with the increased serum IgG1 levels, GCs in *Malt1*$^{PD/PD}$

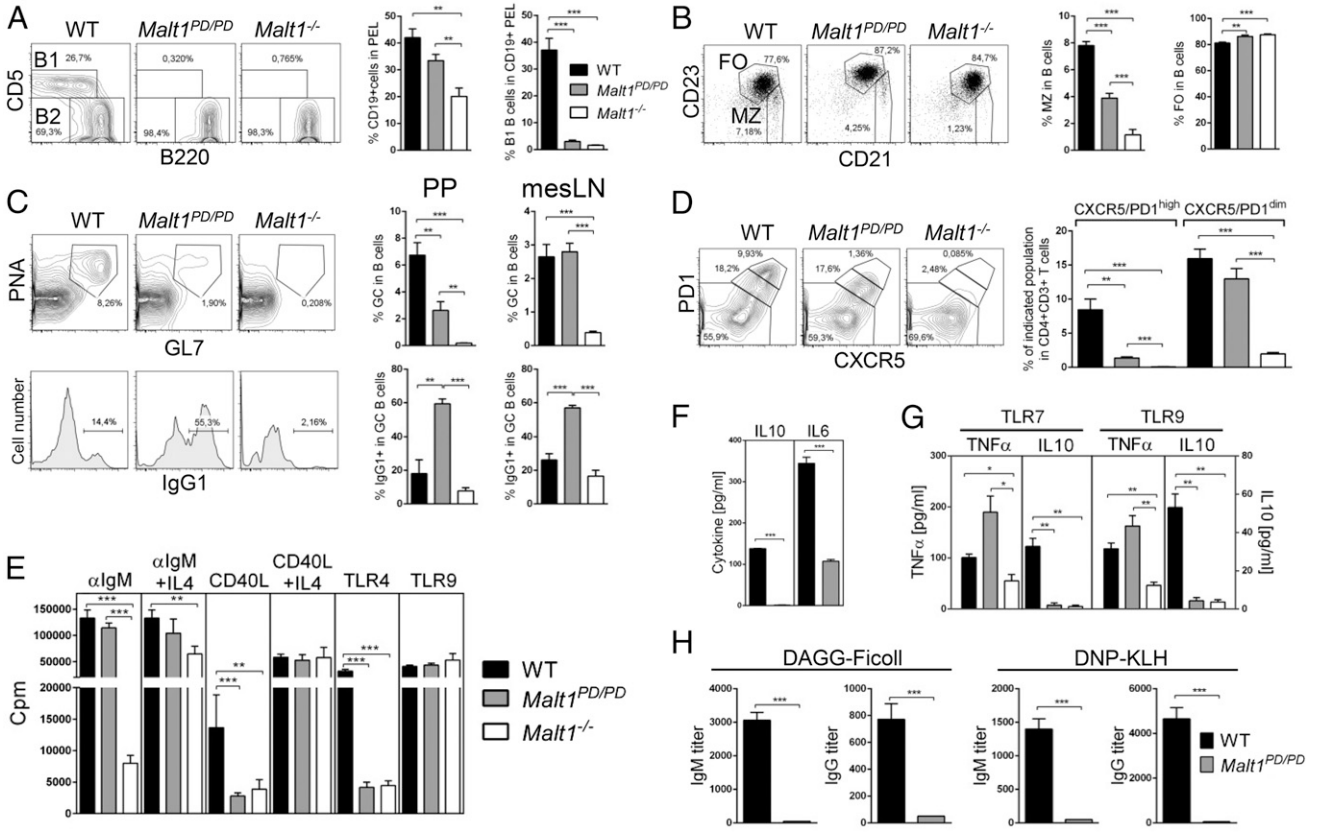

FIGURE 3. Immune alterations in major B cell compartments and defective B cell responses in *Malt1*$^{PD/PD}$ and *Malt1*$^{-/-}$ mice. (**A**) Proportions of B1 versus B2 B cells in PEL. Representative staining after gating on CD19^{+}CD11b^{neg} cells. (**B**) Proportions of MZ versus FO B cells in spleen. Representative stainings and gating strategy based on CD21 and CD23 expression in CD19^{+}B220^{+} B cells. (**C**) Representative staining and proportions of GC B cells in PP after gating on CD19^{+}B220^{+} B cells. Histograms display surface IgG1^{+} in the GC B cell gate in PP and mesLN. (**D**) Representative staining of T_{FH} in PP after gating on CD3^{+}CD4^{+} T cells. T_{FH} cells were divided in CXCR5/PD1^{high} and CXCR5/PD1^{dim}. (A–D) Data are representative of at least three independent experiments. Data in bar graphs are mean ± SEM ($n = 5$ per group). (**E**) [^{3}H]thymidine incorporation of purified WT, *Malt1*$^{PD/PD}$, or *Malt1*$^{-/-}$ B cells activated in vitro by different stimuli for 3 d. (**F**) Reduced production of IL-10 and IL-6 after overnight stimulation of FACS-sorted *Malt1*$^{PD/PD}$ MZ B cells with the TLR9 ligand CpG1826. Bars represent mean ± SEM of technical replicates data obtained on sorted MZ B cells after sorting of pooled spleens from at least three mice per group. Data are representative of two independent experiments. (**G**) Altered TNF-α, IL-6, and IL-10 secretion by *Malt1*$^{PD/PD}$ and *Malt1*$^{-/-}$ splenic B cells after overnight stimulation with TLR7 or TLR9 ligands. Bars represent mean ± SEM of data obtained on B cells from three independent mice per group and a representative of two independent experiments. (**H**) Anti-DNP IgM and IgG titers after immunization with DNP-KLH or DAGG-Ficoll. Anti-DNP Ab titers were assessed 8 d after DNP-KLH immunization and 6 d after DAGG-Ficoll immunization. Data are representative of two independent experiments on $n = 5$ mice/group. In all graphs statistical significance was calculated using a two-tailed unpaired t test (*$p < 0.05$, **$p < 0.01$, ***$p < 0.001$).

mice contained increased proportions of IgG1^{+} B cells (Fig. 3C, Supplemental Fig. 3D). Similarly to the GC B cell population, the T_{FH} compartment was only partially reduced in *Malt1*$^{PD/PD}$ mice with a selective abrogation of CXCR5/PD1^{high} T_{FH} cells, but detectable levels of CXCR5/PD1^{dim} T_{FH} cells (Fig. 3D). Thus, although the combined absence of the scaffolding and enzymatic functions of MALT1 severely abrogated the generation of innate B1, MZ B cells, T_{FH}, and GC B cells, the selective lack of MALT1 enzymatic activity disrupted the B1 B cell compartment, but only partially affected the MZ, GC B cells, and T_{FH} cells.

To better understand the relevance of MALT1 proteolytic activity on B cell function, we assessed in vitro proliferative responses of purified splenic B cells in response to major triggers such as BCR, CD40, and TLR agonists. After IgM, TLR4, or CD40 triggering, proliferation of *Malt1*$^{-/-}$ B cells was significantly reduced (Fig. 3E). For anti-IgM and anti-CD40 stimulation, the defects were partially rectified by addition of exogenous IL-4. *Malt1*$^{PD/PD}$ B cells also showed defective proliferation in response to activation through TLR4 and CD40, but not by anti-IgM (Fig. 3E). Similarly to *Malt1*$^{-/-}$ B cells, addition of IL-4 restored the proliferation of *Malt1*$^{PD/PD}$ B cells in response to CD40 stimulation. TLR9-induced proliferation of B cells from *Malt1*$^{-/-}$ and *Malt1*$^{PD/PD}$ was normal.

Although *Malt1*$^{PD/PD}$ mice had a detectable MZ B cell population, ex vivo restimulation of MZ B cells with a TLR9 agonist revealed that the *Malt1*$^{PD/PD}$ MZ B cells did not produce IL-10 and secreted lower levels of IL-6 (Fig. 3F). Similar defects in IL-10 production, but normal or enhanced production of TNF-α was observed after ex vivo stimulation of total purified *Malt1*$^{PD/PD}$ splenic B cells (Fig. 3G), suggesting that certain immunoregulatory functions of MZ-like B cells are also abrogated in the absence of the proteolytic activity of MALT1.

The multiple defects characterizing the T_{FH} and B cell compartments of *Malt1*$^{-/-}$ mice have been associated with defective B cell responses to TD and TI-2 Ags (8, 9), a finding we could confirm (Supplemental Fig. 3E). *Malt1*$^{PD/PD}$ mice were also unable to mount IgM and IgG responses when immunized with the TI-2 Ag DAGG-Ficoll (Fig. 3H). Interestingly, *Malt1*$^{PD/PD}$ mice also displayed abrogated Ab responses to the TD Ag DNP-KLH conjugate. The reduced signaling through CD40 combined with reduced T_{FH} cell proportions likely contributed to the defective TD B cell responses observed in *Malt1*$^{PD/PD}$ mice.

Catalytic inactivation of MALT1 increases the frequency of effector T cells and alters the cytokine expression profile

In view of the partial impact of the MALT1 C472A mutation on T_{FH} differentiation, we next analyzed the composition and function of other T cell subsets present in lymphoid organs. *Malt1*$^{PD/PD}$ mice displayed a partial reduction in the proportion of CD4$^+$ and CD8$^+$ T cells (Supplemental Fig. 3F), mainly in LN displaying increased cellularity (i.e., mesLN and cerLN). Of note, proportions of effector memory (T_{EM}) and central memory (T_{CM}) CD4$^+$ and CD8$^+$ T cells in LN and spleen of *Malt1*$^{PD/PD}$ mice were increased (Fig. 4A and data not shown). A similar increase in CD44 levels and the T_{CM} subtype was also apparent in *Malt1*$^{-/-}$ mice.

The functional ex vivo characterization of splenic T cells indicated that *Malt1*$^{-/-}$ T cells displayed severely impaired proliferative responses after activation by CD3 and CD28 Abs (Fig. 4B), confirming previous findings (8, 9). By contrast, [^{3}H]thymidine incorporation by *Malt1*$^{PD/PD}$ T cells was reduced compared with WT cells, but not to the extent observed for *Malt1*$^{-/-}$ T cells. Previous work using T cell lines reconstituted with an enzymatically inactive form of MALT1 suggested that the proteolytic function of MALT1 was important for TCR-triggered IL-2 production, a major survival factor required for in vitro T cell proliferation (11). Consistent with this, we observed that *Malt1*$^{PD/PD}$ CD4$^+$ and CD8$^+$ T cells produced lower amounts of IL-2 and TNF-α after ex vivo restimulation with PMA/ionomycin (Fig. 4C and 4D). Once again, defects of *Malt1*$^{-/-}$ T cells were more profound than those of *Malt1*$^{PD/PD}$ T cells.

Optimal production of IL-2 and TNF-α relies on the activity of the NF-κB member c-Rel (23, 24). MALT1 substrates such as RelB and Regnase-1 can impact the activity and expression of c-Rel and IL-2 either by modulating c-Rel localization or by promoting c-Rel and IL-2 mRNA degradation, respectively (16, 17). Consistent with the accumulation of uncleaved RelB and Regnase-1 detected in PMA/ionomycin-activated *Malt1*$^{PD/PD}$ and *Malt1*$^{-/-}$ T cells (Fig. 1A), *Malt1*$^{PD/PD}$ and *Malt1*$^{-/-}$ T cells failed to upregulate the mRNAs encoding for c-Rel and IL-2 upon activation (Fig. 4E).

Collectively, the accumulation of uncleaved MALT1 substrates in *Malt1*$^{PD/PD}$ T cells was sufficient to indirectly impact expression of certain activation-induced genes resulting in defective production of cytokines such as IL-2 and TNF-α and leading to partially impaired proliferative responses in vitro. The normal activation of the MALT1 scaffolding function-dependent IKK axis combined with the defective modulation of c-Rel activity and Regnase-1–regulated genes might lead to an imbalanced immune homeostasis.

Functional defects in Malt1$^{PD/PD}$ *T cells lead to EAE resistance and skewed Th1 and Th2 responses in vivo*

The enhanced cerLN and mesLN size and accumulation of memory T cells in lymphoid organs of *Malt1*$^{PD/PD}$ mice indicated that T cell activation and expansion in vivo occurred irrespective of the defective IL-2 and TNF-α production identified in vitro. Interestingly, the cytokine expression pattern of spleen cells stimulated with PMA/ionomycin ex vivo revealed higher amounts of the Th1 cytokine IFN-γ and strongly elevated Th2 cytokines such as IL-4 and IL-13 in *Malt1*$^{PD/PD}$ splenocytes (Fig. 4D). These data suggested that the immune defects associated with selective deficiency of MALT1 proteolytic activity were associated with the expansion of both Th1- and Th2-skewed T cells in vivo.

In view of the Th1- and Th2-skewed T cell responses observed in *Malt1*$^{PD/PD}$ mice and the previously reported defective differentiation of *Malt1*$^{-/-}$ T cells into Th17 cells (25), we investigated the Th1 and Th17 differentiation potential of *Malt1*$^{PD/PD}$ T cells. In vitro skewing of *Malt1*$^{PD/PD}$ and *Malt1*$^{-/-}$ CD4$^+$ T cells toward Th1 cells was normal (Fig. 5A). By contrast, *Malt1*$^{PD/PD}$ and *Malt1*$^{-/-}$ CD4$^+$ T cells displayed a severe reduction in IL-17 production after differentiation into Th17 cells (Fig. 5A). With the aim to further elucidate the relevance of defective Th17 differentiation in vivo, we analyzed *Malt1*$^{PD/PD}$ mice in a Th17-dependent EAE model. Consistent with our in vitro findings, *Malt1*$^{PD/PD}$ mice were completely protected from EAE development induced by immunization with MOG_{1-125} in adjuvant (Fig. 5B).

Overall, the lack of MALT1 protease activity in T cells altered the activation process and cytokine expression profile of T cells induced upon stimulation. Although IL-2, TNF-α, and IL-17 production were reduced or impaired, secretion of IFN-γ and Th2 cytokines was not affected. The IL-4– and IL-13–rich environment identified in lymphoid organs of *Malt1*$^{PD/PD}$ mice also suggested that Th2-skewed responses promoted the IgG1 and IgE B cell responses observed in these mice.

Reconstitution of Malt1$^{PD/PD}$ *mice with WT Tregs overcomes a partial Treg deficiency and delays the multiorgan inflammatory pathology*

The spontaneous and progressive pathology characterizing *Malt1*$^{PD/PD}$ mice shared many similarities with the disease occurring in certain mouse strains characterized by an impaired Treg compartment. The CBM complex is critical for the development and survival of natural Treg cells, and *Malt1*$^{-/-}$ mice were previously reported to display a severe impairment in peripheral Tregs (26–28). Whereas *Malt1*$^{-/-}$ mice displayed the expected severe reduction in Foxp3$^+$ Tregs (Fig. 6A), *Malt1*$^{PD/PD}$ mice were characterized by an ~60% decrease in Foxp3$^+$ cells in the CD4$^+$ T cell compartment compared with WT littermate controls in all lymphoid organs tested (Fig. 6A). In vitro Treg differentiation experiments performed in the presence of exogenous IL-2 indicated that *Malt1*$^{PD/PD}$ CD4 T cells have the potential to differentiate into Tregs (Fig. 6B).

Considering the reduced Treg proportions and the functional alterations of *Malt1*$^{PD/PD}$ T cells and B cells, we hypothesized that the spontaneous multiorgan pathology occurring in *Malt1*$^{PD/PD}$ mice developed as a result of improper Treg-mediated suppression. To test this, we adoptively transferred WT Tregs isolated from EGFP-Foxp3 animals into *Malt1*$^{PD/PD}$ mice. The transfer of 0.5×10^6 WT Tregs into female *Malt1*$^{PD/PD}$ mice delayed the weight loss and the lethal phenotype (Fig. 6C). By contrast, *Malt1*$^{PD/PD}$ mice receiving PBS or WT EGFP^{neg}CD4$^+$Foxp3^{neg} cells displayed the typical symptoms and started to succumb to the immune pathology.

A major role of the defective Treg compartment in the development of the spontaneous pathology was also supported by additional observations made in BM chimeric mice in which sublethally irradiated CD45.1$^+$ WT recipients were reconstituted with CD45.2$^+$ BM cells from WT or *Malt1*$^{PD/PD}$ mice. Interestingly, the recipient mice receiving *Malt1*$^{PD/PD}$ BM cells were characterized by similar defects in immune compartments to those observed in *Malt1*$^{PD/PD}$ mice (Supplemental Fig. 4A–D). However, none of the *Malt1*$^{PD/PD}$ BM chimeras developed any of the symptoms of pathology occurring in constitutive *Malt1*$^{PD/PD}$ mice. All animals did not develop any sign of hypercellularity, multiorgan T and B cell infiltration, T_{EM} and T_{CM} cell expansion, or increased IgG1 and IgE levels for up to 38 wk after reconstitution (Supplemental Fig. 4E–H and data not shown). As expected, the majority of the CD4$^+$ and CD8$^+$ T cell, B cell, and myeloid compartments were derived from the BM donor cells (Supplemental Fig. 4E–G). Remarkably, WT Tregs derived from

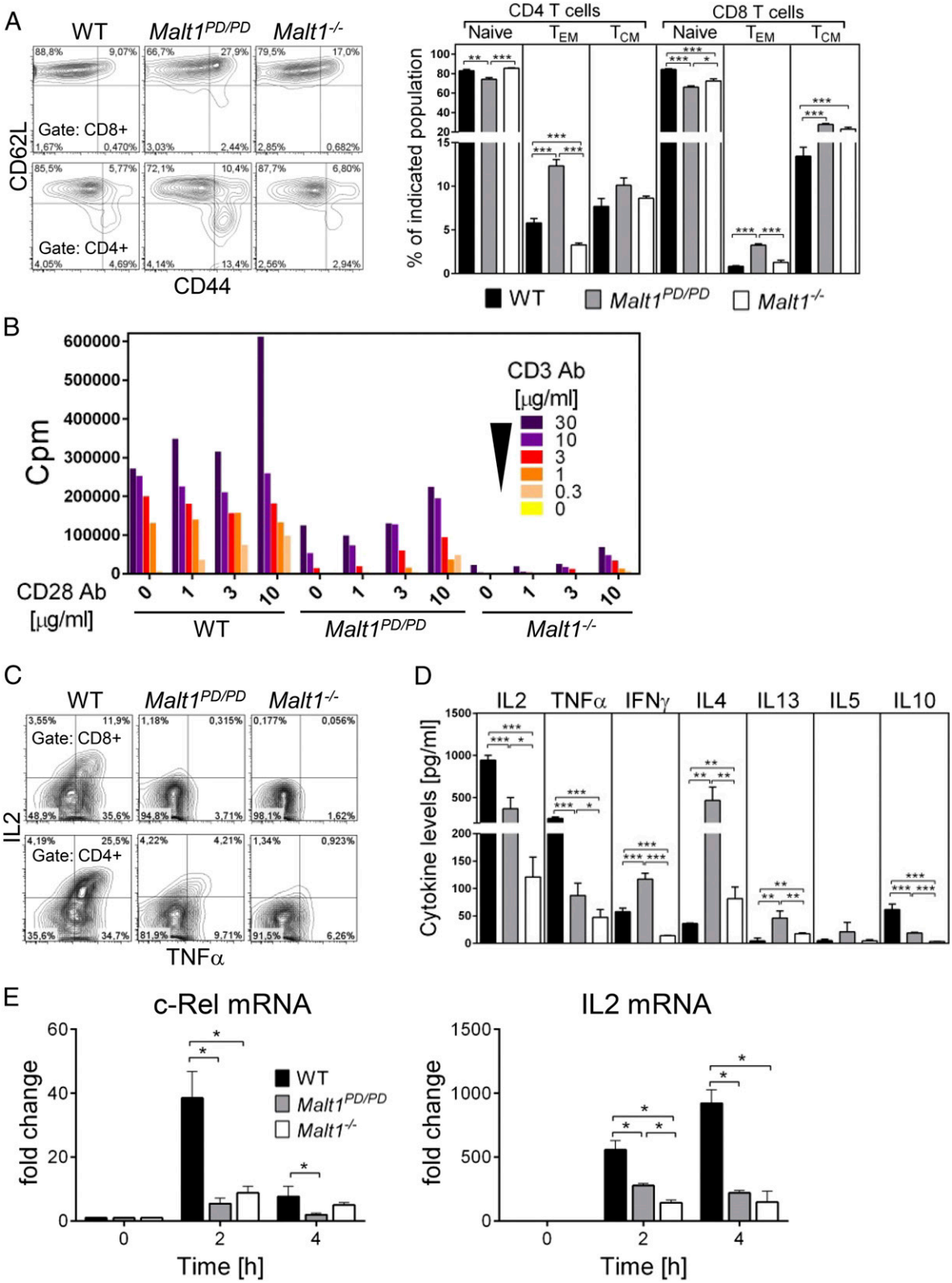

FIGURE 4. Dysfunctional responses of *Malt1*$^{PD/PD}$ and *Malt1*$^{-/-}$ T cells including reduced IL-2 and TNF-α. (**A**) Representative staining and proportions of naive, CD44^{high}CD62L^{low} T_{EM}, and CD44^{high}CD62L^{high} T_{CM} subset distribution among CD8$^+$ and CD4$^+$ T cell populations present in cerLN. Bars represent mean ± SEM ($n = 5$ mice/group). Data are representative of three independent experiments. (**B**) Proliferation of purified *Malt1*$^{PD/PD}$ and *Malt1*$^{-/-}$ CD3$^+$ T cells stimulated with different concentrations of plate-bound CD3 and CD28 Abs. Data are representative of two independent experiments. (**C**) Intracellular cytokine staining of LN CD4$^+$ and CD8$^+$ T cells stimulated ex vivo for 4 h with PMA/ionomycin. (**D**) Cytokine expression pattern of spleen cells stimulated ex vivo for 4 h with PMA/ionomycin. Bars represent mean ± SEM of data obtained on spleen cells from three independent mice per group and a representative of two independent experiments. (**E**) Modulation of c-Rel and IL-2 mRNA levels in WT, *Malt1*$^{-/-}$, and *Malt1*$^{PD/PD}$ purified splenic CD4$^+$ T cells. mRNA levels were evaluated by Q-PCR at different times after PMA/ionomycin stimulation. The mRNA expression level was normalized to the expression level of β_2-microglobulin, and fold changes were calculated using the ΔΔ cycle threshold method. Bars indicate average ± SD. Data are representative of at least two independent experiments. Statistical significance was calculated using a two-tailed unpaired *t* test (*$p < 0.05$, **$p < 0.01$, ***$p < 0.001$).

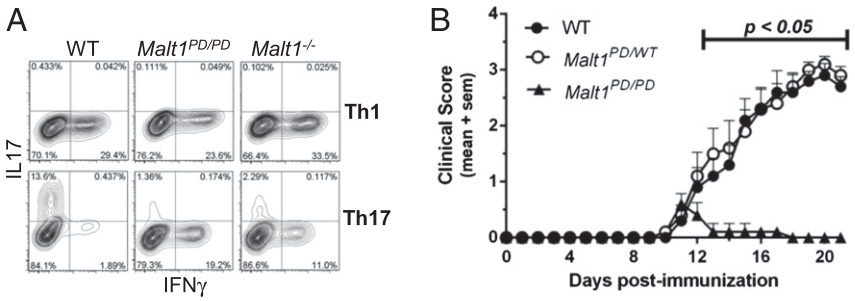

FIGURE 5. Functional defects of *Malt1*$^{PD/PD}$ and *Malt1*$^{-/-}$ T cells result in defective Th17 differentiation and protection in an EAE model. (**A**) In vitro Th1 and Th17 differentiation of naive CD4$^+$ T cells. Seventy-two hours after in vitro differentiation, Th cells were restimulated for 6 h with PMA/ionomycin followed by intracellular cytokine staining. (**B**) WT, *Malt1*$^{PD/WT}$, and *Malt1*$^{PD/PD}$ mice were immunized with $MOG_{1–125}$ in CFA. EAE clinical score was assessed daily. The experiment included 10 mice/group. Statistical significance was determined by Kruskal–Wallis one-way ANOVA.

the CD45.1$^+$ recipient accounted for ~80% of the Treg repertoire of the chimeras reconstituted with the *Malt1*$^{PD/PD}$ BM cells compared with ~20% of the Treg compartment in chimeras receiving WT BM cells (Supplemental Fig. 4I). These data highlighted that a fraction of the recipient's Treg compartment survived the sublethal irradiation process and probably had a survival and/or homeostatic proliferation advantage over the Tregs derived from the *Malt1*$^{PD/PD}$ hematopoietic precursors. In line with the Treg adoptive transfer data, the presence of WT Treg likely prevented disease development despite the immune defects characterizing the *Malt1*$^{PD/PD}$ hematopoietic compartment.

Therefore, these data strongly suggest that the immune defects and partial Treg deficiency characterizing *Malt1*$^{PD/PD}$ mice, combined with the capacity to mount certain types of T cell and B cell immune responses, contribute to the development of the multiorgan inflammatory pathology observed.

Discussion

In this study, we investigated the relative contributions of the protease versus scaffolding functions of the paracaspase MALT1 in the regulation of T and B cell immune function in vivo by characterizing novel MALT1 PD mice (*Malt1*$^{PD/PD}$) and comparing them with *Malt1*$^{-/-}$ mice. Our findings indicated that the selective lack of MALT1 protease activity prevented the formation of a functional peritoneal B1 B cell compartment and led to defective CD40 and TLR4 signaling in B cells, defective TLR9-induced IL10 production by MZ B cells, and defective Th17 differentiation. In addition, *Malt1*$^{PD/PD}$ mice were unable to mount B cell responses to TD and TI-2 Ags and were protected in a Th17-dependent EAE model similarly to *Malt1*$^{-/-}$ mice. By contrast, MALT1 proteolytic activity only partially affected other immune cell subsets and functions. This was highlighted first by the development of MZ B cells, which was relatively undisturbed in

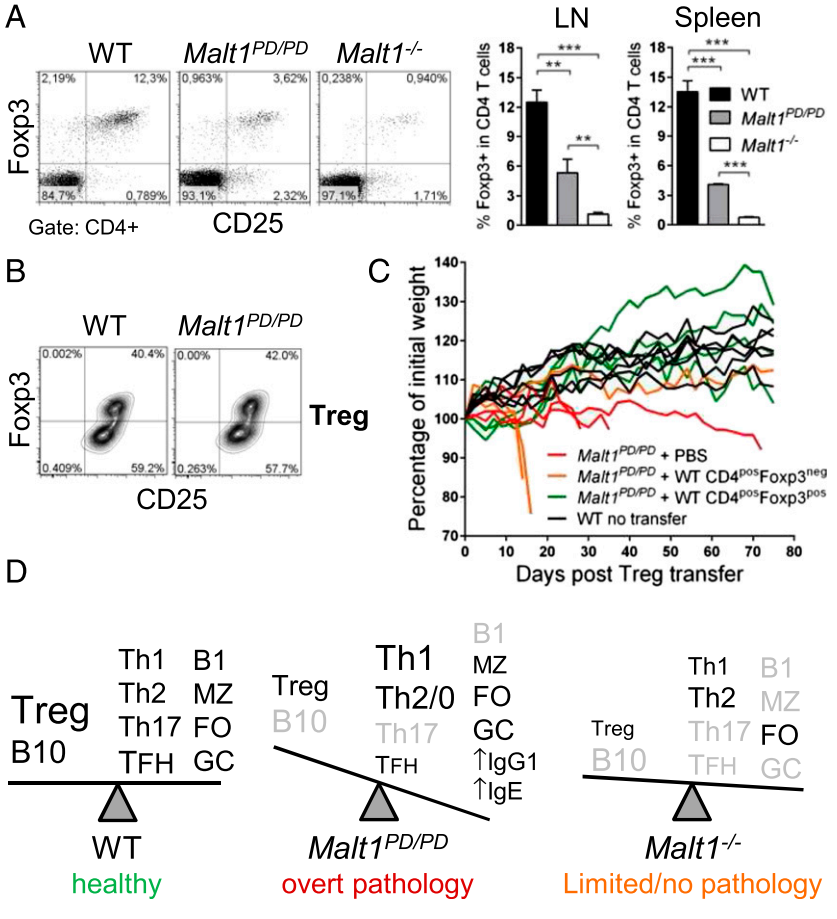

FIGURE 6. Reconstitution of *Malt1*$^{PD/PD}$ mice with WT Treg delays disease development. (**A**) Representative CD25 versus Foxp3 staining of CD4$^+$ T cells from cerLN. Bars indicate the proportion of Foxp3$^+$ cells among CD4$^+$ T cells and represent mean ± SEM (n = 5 mice/group). Data are representative of three independent experiments. $^{**}p < 0.01$, $^{***}p < 0.001$. (**B**) In vitro Treg differentiation of naive CD4$^+$ T cells. Analyses were performed 72 h after in vitro differentiation. (**C**) Adoptive transfer of WT EGFP$^+$Foxp3$^+$CD4$^+$ Treg into 8- to 9-wk-old *Malt1*$^{PD/PD}$ mice prevents early lethality and delays weight loss. Data are representative of two independent experiments with three to five animals per group. (**D**) Schematic representation of unbalanced immune homeostasis in *Malt1*$^{PD/PD}$ and *Malt1*$^{-/-}$ mice. Immune homeostasis is maintained in WT animals by a balance between immunoregulatory cell types such as Tregs and IL-10–producing MZ-like B cells (B10) and appropriate Th and B cell responses. In *Malt1*$^{PD/PD}$ mice, reduced Tregs and defective IL-10 production by B10 cells combined with partially defective T cell and B cell immunity tilts the balance toward the effector cell side leading to a spontaneous multiorgan pathology associated with the expansion of Th0, Th1, and Th2 effector cells. Despite a severe Treg and B10 B cell deficiency, *Malt1*$^{-/-}$ mice do not display overt pathology because of the more severe functional defects in T cells and B cells that counterbalance the lack of immunoregulatory cells.

Malt1$^{PD/PD}$ but defective in *Malt1*$^{-/-}$ mice. Second, T_{FH} and GC B cell compartments were only moderately diminished in *Malt1*$^{PD/PD}$ animals, but completely abrogated in *Malt1*$^{-/-}$ mice. Third, *Malt1*$^{PD/PD}$ T cells displayed a milder defect in proliferative responses and in IL-2 and TNF-α production compared with *Malt1*$^{-/-}$ T cells. These defects were associated with subtle alterations in NF-κB activation observed in *Malt1*$^{PD/PD}$ T cells in contrast with the severe abrogation detected in *Malt1*$^{-/-}$ T cells. Finally, natural Treg proportions in the CD4$^+$ T cell compartment were reduced by ~60% in *Malt1*$^{PD/PD}$ mice, but were almost completely absent in *Malt1*$^{-/-}$ mice. Unexpectedly, we found that the immune alterations associated with the selective absence of MALT1 protease function resulted in a lethal inflammatory pathology associated with accumulation of T_{EM} and T_{CM} CD4$^+$ and CD8$^+$ T cells in lymphoid organs, Th1- and Th2-skewed responses, enhanced IgG1 and IgE levels, and lymphocytic infiltrations in multiple organs.

The pathology observed in the *Malt1*$^{PD/PD}$ mouse is reminiscent of the phenotype associated with partial or complete reduction in Treg numbers due to defective IL-2 signaling or Foxp3 deficiency (29–34). However, the pathology of *Malt1*$^{PD/PD}$ mice was associated with a slower onset, mandibular- and mesLN-restricted lymphadenopathy, and lymphocytic infiltration in a more limited set of organs. Because TCR- and CD28-mediated signals, as well as IL-2 levels, are important for natural Treg development and peripheral survival, it is likely that the alteration of CBM-driven signaling events and the incomplete abrogation of IL-2 production we observed in *Malt1*$^{PD/PD}$ T cells contributed to the partial deficiency in Foxp3$^+$ Treg cells in the *Malt1*$^{PD/PD}$ CD4 T cell compartment. In line with a Treg development defect, we observed a reduction in the Foxp3$^+$ Treg proportions also among *Malt1*$^{PD/PD}$ CD4 single-positive thymocytes (data not shown).

The potential association between an imbalanced Treg compartment and the inflammatory pathology in *Malt1*$^{PD/PD}$ mice was supported by the delay in symptoms of disease after reconstitution of *Malt1*$^{PD/PD}$ mice with WT Tregs. Although the Treg transfer was sufficient to delay weight loss and the appearance of symptoms over the observation time, histopathology analyses performed on the various animals at the time of sacrifice revealed no or only limited reduction of the inflammatory infiltrates and cerLN cellularity (data not shown). We believe that the reason for limited histopathological amelioration is related to the pre-existing asymptomatic pathology already present in the mice at time of the Treg transfer. The different ages at which the animals were analyzed (i.e., most of the Treg transferred mice were analyzed at later time points than the other groups) may account as well. Altogether, these conditions may limit the overall effect of the Treg transfer. However, additional experiments involving BM chimeras bearing a *Malt1*$^{PD/PD}$ hematopoietic system suggested that WT Tregs surviving the sublethal irradiation of recipient animals likely prevented disease development despite the immune defects in the *Malt1*$^{PD/PD}$ hematopoietic compartment. In line with this, radiation-resistant Tregs were reported previously to prevent T cell–mediated autoimmunity after syngeneic BM transplantation (35). Detailed histopathology analyses revealed only limited effects on nonimmune cells, but we cannot fully exclude that additional alterations outside the hematopoietic compartment also contribute to disease development in *Malt1*$^{PD/PD}$ mice. More specific analyses in affected peripheral tissues are required to investigate this question.

In contrast with *Malt1*$^{PD/PD}$ mice, *Malt1*$^{-/-}$ mice displayed an almost complete absence of peripheral Tregs, yet did not develop any overt sign of immune pathology. Of note, we did observe mild lymphadenopathy of mesLN and cerLN and an increased proportion of T_{CM}-like cells in the lymphoid organs of *Malt1*$^{-/-}$ mice, as well as moderate lymphoid cell infiltration in lacrimal and salivary glands (data not shown). In line with the critical role of CBM-driven signals and IL-2 in promoting Treg development and survival, *Malt1*$^{-/-}$ T cells displayed a more severe abrogation of CBM-mediated NF-κB activation resulting in strongly impaired IL-2 and TNF-α production. Therefore, although abrogation of the Treg compartment in *Malt1*$^{-/-}$ animals potentially sensitized them to develop a similar pathology as *Malt1*$^{PD/PD}$ mice, the more severe functional defects in the T and B cell compartments likely limited the expansion and activation of pathogenic effector cells and restrained the extent and severity of the disease. In contrast, we believe that the pathology occurring in *Malt1*$^{PD/PD}$ mice was facilitated by the combination of impaired immunosuppressive compartments (e.g., Treg and IL-10–producing B cells) and partially dysfunctional T and B cells, which retained the capacity to generate Th1- and Th2-skewed effectors in response to yet unidentified Ags (Fig. 6D). Interestingly, analyses involving FACS-based intracellular cytokine staining aiming at assessing the identity of IL-4– and IFN-γ–producing cells suggest that the main sources of these cytokines among *Malt1*$^{PD/PD}$ T cells are CD44^{high} T_{EM} and T_{CM} CD8$^+$ cells of a Th1-like phenotype (IFN-γ$^+$IL4$^-$) and CD44^{high} T_{EM} and T_{CM} CD4$^+$ cells including a mix of Th0 (IFN-γ$^+$IL4$^+$), Th1 (IFN-γ$^+$IL4$^-$), and Th2 (IFN-γ$^-$IL4$^+$) phenotypes (data not shown). Given the accumulation of these multiple T cell subsets, additional work will be required to assess how these different subsets contribute to the complex multiorgan pathology occurring in *Malt1*$^{PD/PD}$ mice and which Ags drive the expansion of these different lymphocyte populations. In addition, given the central defect in thymic Treg development observed in *Malt1*$^{PD/PD}$ mice, it remains to be assessed whether alterations in the thymic selection process associated with defective MALT1 proteolytic activity may also promote pathology development by releasing autoreactive T cell clones (normally deleted in WT animals) in the peripheral T cell effector pool.

The accumulation of IL-4– and IL-13–producing Th0/Th2 cell subsets in *Malt1*$^{PD/PD}$ mice was also highlighted by increased CD23 (FcεRII) levels on FO and MZ B cells (Fig. 3B, Supplemental Fig. 3B). Indeed, IL-4, IL-13, and IgE were previously reported to upregulate CD23 expression (discussed by Dierks et al. [36]). The Th2-skewing observed in *Malt1*$^{PD/PD}$ mice may also explain the enhanced IgG1 and IgE levels observed in these animals. However, it was intriguing to observe that *Malt1*$^{PD/PD}$ mice could not mount Ab responses to TD and TI-2 Ags upon immunization. Further investigation is required to assess whether endogenous GC B cell responses and IgG1 and IgE secretion rely on help provided by the CXCR5/PD1^{dim} T_{FH} cells remaining in *Malt1*$^{PD/PD}$ mice, or whether alternative T cell–independent pathways also contribute to this process (37). Innate B1 and MZ B cells are key mediators of TI-2 B cell responses (38). Because DAGG-Ficoll was administered in the absence of additional adjuvants, we believe that the defective anti-DNP IgM and IgG responses observed in *Malt1*$^{PD/PD}$ mice were a consequence of the absent B1 B cells and reduced/dysfunctional MZ B cell compartment observed in these mice. It is therefore likely that the GC B cells retained in mesLN and PP of *Malt1*$^{PD/PD}$ mice are directed to other types of Ags present at these sites and triggering alternative B cell costimulatory pathways independent of MALT1 protease activity such as TLR7 or TLR9 agonists associated with, for example, TI-1 Ags present in the intestinal microflora.

The selective effect on cytokines such as IL-2, TNF-α, and IL-17, and the expansion of Th1-like IFN-γ$^+$ T cells, as well as Th0/Th2 cytokine-producing cells, observed in *Malt1*$^{PD/PD}$ mice sug-

gests that MALT1 protease function modulates selected transcriptional programs downstream of the TCR. Our analysis of the signaling events downstream of the CBM complex revealed minor changes in IκBα, p65, or p105 phosphorylation and IκBα degradation in both *Malt1*$^{PD/PD}$ T cells and B cells. This suggests that MALT1 protease activity modulates signaling events downstream of the CBM complex without completely abrogating canonical NF-κB signaling (via the IKK-IκB axis). It is interesting to observe that the alterations in the T and B cell compartments identified in *Malt1*$^{PD/PD}$ mice closely resemble those reported in c-Rel–deficient animals (23, 39–42). Moreover, c-Rel was also shown to regulate IL-21 production and T_{FH} cell differentiation (43). These similarities are consistent with recent reports showing that cleavage of RelB and Regnase-1 by MALT1 can influence c-Rel levels and activity (16, 17). Our biochemical analyses could demonstrate the accumulation of uncleaved RelB and Regnase-1 in *Malt1*$^{PD/PD}$ T cells and B cells. Consistent with this, analysis of the levels of several Regnase-1–regulated mRNA in T cells clearly indicated that c-Rel as well as IL-2 mRNA induction was abrogated in the absence of MALT1 proteolytic activity. These data strongly indicate that reduced c-Rel–mediated transcription contributed to the functional defects identified in *Malt1*$^{PD/PD}$ T cells. However, the lack of overt inflammatory pathology in c-Rel–deficient mice indicates that additional defects contribute to the pathology characterizing *Malt1*$^{PD/PD}$ animals.

In conclusion, this work revealed a previously unappreciated role for the MALT1 protease activity in finely regulating immune function and homeostasis. The defective Th17 and B cell responses observed in *Malt1*$^{PD/PD}$ mice highlight the therapeutic potential of drugs targeting MALT1 protease function. In line with this, treatment with mepazine, which inhibits MALT1 protease activity in a micromolar range, was recently reported to attenuate EAE symptoms (44). However, the reduced Treg compartment and multiorgan pathology occurring in *Malt1*$^{PD/PD}$ mice provide a warning for the potential risks associated with sustained abrogation of MALT1's enzymatic activity. Development of inducible PD mice or selective MALT1 inhibitors will help clarify whether chronic inhibition of MALT1 activity in autoimmune pathologies is of therapeutic value. The spontaneous pathology and the complexity of the immune alterations identified in this study open new exciting questions that deserve further investigation. In particular, it is still unclear which Ags and pathways drive the accumulation of T_{EM} and T_{CM} cells and the IgG1/IgE-skewed B cell responses in *Malt1*$^{PD/PD}$ mice, and what is their contribution to the overall pathology. More importantly, what is the relevance of MALT1 protease activity in humans? Polymorphisms in the *Malt1* gene have been associated with combined immunodeficiency (45–47). However, in all cases the mutations resulted in a complete deficiency of the protein or very low MALT1 levels because of protein instability. Further work is required to assess whether specific mutations in the catalytic function of MALT1 contribute to multiorgan inflammatory disorders.

Note added in proof. During the revision of this manuscript, two studies reporting the generation and characterization of novel *Malt1*$^{PD/PD}$ mouse lines were published (48, 49). Both articles described *Malt1*$^{PD/PD}$ mice characterized by cerLN and mesLN lymphadenopathy and very similar immune defects to the ones we describe in our manuscript. Jaworski et al. (48) claim that *Malt1*$^{PD/PD}$ mice succumb to autoimmune gastritis and provide evidence that the disease can be prevented by the adoptive transfer of WT Tregs into 3- to 8-d-old *Malt1*$^{PD/PD}$ mice. Gewies et al. (49) describe an inflammatory pathology characterized by lymphocytic infiltrates in the glandular stomach but also a neurological disorder associated with dystonia and progressive ataxia that was prevented by a deficiency in Bcl10, T and B cell compartments (Rag1KO mice), or IFN-γ production.

Acknowledgments

We thank Patricia Brander Weber for the initial histopathological evaluations as well as Daniele Anastasi, Maureen Bardet, Karine Bigot, Vanessa Cornacchione, Elena Degl'Innocenti, Nicolas Dubois, Esther Erard, Yvonne Hager, Catherine Huck, Bernhard Jost, David Ledieu, Daniel Kaiser, Sonja Kerstin Frentzel, Bernadette Kleylein-Sohn, Claire Malinverni, Barbara Metzler, Gautier Robert, Regina Santoro, Philippe Scheubel, Patrick Schmutz, Pamela Ramseier, Roland Sollberger, Marie-Catherine Stutz, Adeline Unterreiner, and Catherine Wioland for excellent technical assistance and additional contributions. We also thank Stephan Gadola, Chauncey Spooner, and Michael W. Tusche for comments and discussions.

Disclosures

F.B., F.R., H.S., R.T., Y.K., I.T.-A., J.S.R., P.A.S., M.B., U.J.-W., C.B., J.D., S.N., A.K., B.N.-H., G.W., G.Z., B.K., E.T., N.Z., C.H.R., D.D.P., and T.C. are employees and/or shareholders of Novartis. The other authors have no financial conflicts of interest.

References

1. Gerondakis, S., T. S. Fulford, N. L. Messina, and R. J. Grumont. 2014. NF-κB control of T cell development. *Nat. Immunol.* 15: 15–25.
2. Perkins, N. D. 2012. The diverse and complex roles of NF-κB subunits in cancer. *Nat. Rev. Cancer* 12: 121–132.
3. Ben-Neriah, Y., and M. Karin. 2011. Inflammation meets cancer, with NF-κB as the matchmaker. *Nat. Immunol.* 12: 715–723.
4. Berger, T., M. E. Saunders, and T. W. Mak. 2013. Dissection of signaling in inflammation: three novel inflammatory regulators. *Cold Spring Harb. Symp. Quant. Biol.* 78: 141–147.
5. Uren, A. G., K. O'Rourke, L. A. Aravind, M. T. Pisabarro, S. Seshagiri, E. V. Koonin, and V. M. Dixit. 2000. Identification of paracaspases and metacaspases: two ancient families of caspase-like proteins, one of which plays a key role in MALT lymphoma. *Mol. Cell* 6: 961–967.
6. Rosebeck, S., A. O. Rehman, P. C. Lucas, and L. M. McAllister-Lucas. 2011. From MALT lymphoma to the CBM signalosome: three decades of discovery. *Cell Cycle* 10: 2485–2496.
7. Wegener, E., and D. Krappmann. 2007. CARD-Bcl10-Malt1 signalosomes: missing link to NF-kappaB. *Sci. STKE* 2007: pe21.
8. Ruland, J., G. S. Duncan, A. Wakeham, and T. W. Mak. 2003. Differential requirement for Malt1 in T and B cell antigen receptor signaling. *Immunity* 19: 749–758.
9. Ruefli-Brasse, A. A., D. M. French, and V. M. Dixit. 2003. Regulation of NF-kappaB-dependent lymphocyte activation and development by paracaspase. *Science* 302: 1581–1584.
10. Fontán, L., and A. Melnick. 2013. Molecular pathways: targeting MALT1 paracaspase activity in lymphoma. *Clin. Cancer Res.* 19: 6662–6668.
11. Rebeaud, F., S. Hailfinger, A. Posevitz-Fejfar, M. Tapernoux, R. Moser, D. Rueda, O. Gaide, M. Guzzardi, E. M. Iancu, N. Rufer, et al. 2008. The proteolytic activity of the paracaspase MALT1 is key in T cell activation. *Nat. Immunol.* 9: 272–281.
12. Coornaert, B., M. Baens, K. Heyninck, T. Bekaert, M. Haegman, J. Staal, L. Sun, Z. J. Chen, P. Marynen, and R. Beyaert. 2008. T cell antigen receptor stimulation induces MALT1 paracaspase-mediated cleavage of the NF-kappaB inhibitor A20. *Nat. Immunol.* 9: 263–271.
13. Malinverni, C., A. Unterreiner, J. Staal, A. Demeyer, M. Galaup, M. Luyten, R. Beyaert, and F. Bornancin. 2010. Cleavage by MALT1 induces cytosolic release of A20. *Biochem. Biophys. Res. Commun.* 400: 543–547.
14. Staal, J., Y. Driege, T. Bekaert, A. Demeyer, D. Muyllaert, P. Van Damme, K. Gevaert, and R. Beyaert. 2011. T-cell receptor-induced JNK activation requires proteolytic inactivation of CYLD by MALT1. *EMBO J.* 30: 1742–1752.
15. Chu, Y., V. Soberon, L. Glockner, R. Beyaert, R. Massoumi, G. van Loo, D. Krappmann, and M. Schmidt-Supprian. 2012. A20 and CYLD do not share significant overlapping functions during B cell development and activation. *J. Immunol.* 189: 4437–4443.
16. Hailfinger, S., H. Nogai, C. Pelzer, M. Jaworski, K. Cabalzar, J. E. Charton, M. Guzzardi, C. Décaillet, M. Grau, B. Dörken, et al. 2011. Malt1-dependent RelB cleavage promotes canonical NF-kappaB activation in lymphocytes and lymphoma cell lines. *Proc. Natl. Acad. Sci. USA* 108: 14596–14601.
17. Uehata, T., H. Iwasaki, A. Vandenbon, K. Matsushita, E. Hernandez-Cuellar, K. Kuniyoshi, T. Satoh, T. Mino, Y. Suzuki, D. M. Standley, et al. 2013. Malt1-induced cleavage of regnase-1 in CD4(+) helper T cells regulates immune activation. *Cell* 153: 1036–1049.
18. Egawa, T., B. Albrecht, B. Favier, M. J. Sunshine, K. Mirchandani, W. O'Brien, M. Thome, and D. R. Littman. 2003. Requirement for CARMA1 in antigen receptor-induced NF-kappa B activation and lymphocyte proliferation. *Curr. Biol.* 13: 1252–1258.

19. Ruland, J., G. S. Duncan, A. Elia, I. del Barco Barrantes, L. Nguyen, S. Plyte, D. G. Millar, D. Bouchard, A. Wakeham, P. S. Ohashi, and T. W. Mak. 2001. Bcl10 is a positive regulator of antigen receptor-induced activation of NF-kappaB and neural tube closure. *Cell* 104: 33–42.
20. Kingeter, L. M., and B. C. Schaefer. 2008. Loss of protein kinase C theta, Bcl10, or Malt1 selectively impairs proliferation and NF-kappa B activation in the CD4+ T cell subset. *J. Immunol.* 181: 6244–6254.
21. Nordin, A. A., and M. H. Schreier. 1982. T cell control of the antibody response to the T-independent antigen, DAGG-Ficoll. *J. Immunol.* 129: 557–562.
22. Pelzer, C., K. Cabalzar, A. Wolf, M. Gonzalez, G. Lenz, and M. Thome. 2013. The protease activity of the paracaspase MALT1 is controlled by monoubiquitination. *Nat. Immunol.* 14: 337–345.
23. Köntgen, F., R. J. Grumont, A. Strasser, D. Metcalf, R. Li, D. Tarlinton, and S. Gerondakis. 1995. Mice lacking the c-rel proto-oncogene exhibit defects in lymphocyte proliferation, humoral immunity, and interleukin-2 expression. *Genes Dev.* 9: 1965–1977.
24. Gerondakis, S., A. Strasser, D. Metcalf, G. Grigoriadis, J. Y. Scheerlinck, and R. J. Grumont. 1996. Rel-deficient T cells exhibit defects in production of interleukin 3 and granulocyte-macrophage colony-stimulating factor. *Proc. Natl. Acad. Sci. USA* 93: 3405–3409.
25. Brüstle, A., D. Brenner, C. B. Knobbe, P. A. Lang, C. Virtanen, B. M. Hershenfield, C. Reardon, S. M. Lacher, J. Ruland, P. S. Ohashi, and T. W. Mak. 2012. The NF-κB regulator MALT1 determines the encephalitogenic potential of Th17 cells. *J. Clin. Invest.* 122: 4698–4709.
26. Huynh, A., R. Zhang, and L. A. Turka. 2014. Signals and pathways controlling regulatory T cells. *Immunol. Rev.* 258: 117–131.
27. Lee, A. J., X. Wu, H. Cheng, X. Zhou, X. Cheng, and S. C. Sun. 2010. CARMA1 regulation of regulatory T cell development involves modulation of interleukin-2 receptor signaling. *J. Biol. Chem.* 285: 15696–15703.
28. Mc Guire, C., P. Wieghofer, L. Elton, D. Muylaert, M. Prinz, R. Beyaert, and G. van Loo. 2013. Paracaspase MALT1 deficiency protects mice from autoimmune-mediated demyelination. *J. Immunol.* 190: 2896–2903.
29. Setoguchi, R., S. Hori, T. Takahashi, and S. Sakaguchi. 2005. Homeostatic maintenance of natural Foxp3(+) CD25(+) CD4(+) regulatory T cells by interleukin (IL)-2 and induction of autoimmune disease by IL-2 neutralization. *J. Exp. Med.* 201: 723–735.
30. Sadlack, B., H. Merz, H. Schorle, A. Schimpl, A. C. Feller, and I. Horak. 1993. Ulcerative colitis-like disease in mice with a disrupted interleukin-2 gene. *Cell* 75: 253–261.
31. Suzuki, H., T. M. Kündig, C. Furlonger, A. Wakeham, E. Timms, T. Matsuyama, R. Schmits, J. J. Simard, P. S. Ohashi, H. Griesser, et al. 1995. Deregulated T cell activation and autoimmunity in mice lacking interleukin-2 receptor beta. *Science* 268: 1472–1476.
32. Willerford, D. M., J. Chen, J. A. Ferry, L. Davidson, A. Ma, and F. W. Alt. 1995. Interleukin-2 receptor alpha chain regulates the size and content of the peripheral lymphoid compartment. *Immunity* 3: 521–530.
33. Sadlack, B., J. Löhler, H. Schorle, G. Klebb, H. Haber, E. Sickel, R. J. Noelle, and I. Horak. 1995. Generalized autoimmune disease in interleukin-2-deficient mice is triggered by an uncontrolled activation and proliferation of CD4+ T cells. *Eur. J. Immunol.* 25: 3053–3059.
34. Malek, T. R. 2008. The biology of interleukin-2. *Annu. Rev. Immunol.* 26: 453–479.
35. Bénard, A., R. Ceredig, and A. G. Rolink. 2006. Regulatory T cells control autoimmunity following syngeneic bone marrow transplantation. *Eur. J. Immunol.* 36: 2324–2335.
36. Dierks, S. E., K. A. Campbell, E. J. Studer, and D. H. Conrad. 1994. Molecular mechanisms of murine Fc epsilon RII/CD23 regulation. *Mol. Immunol.* 31: 1181–1189.
37. Vinuesa, C. G., and P. P. Chang. 2013. Innate B cell helpers reveal novel types of antibody responses. *Nat. Immunol.* 14: 119–126.
38. Martin, F., A. M. Oliver, and J. F. Kearney. 2001. Marginal zone and B1 B cells unite in the early response against T-independent blood-borne particulate antigens. *Immunity* 14: 617–629.
39. Chen, G., K. Hardy, E. Pagler, L. Ma, S. Lee, S. Gerondakis, S. Daley, and M. F. Shannon. 2011. The NF-κB transcription factor c-Rel is required for Th17 effector cell development in experimental autoimmune encephalomyelitis. *J. Immunol.* 187: 4483–4491.
40. Deenick, E. K., A. R. Elford, M. Pellegrini, H. Hall, T. W. Mak, and P. S. Ohashi. 2010. c-Rel but not NF-kappaB1 is important for T regulatory cell development. *Eur. J. Immunol.* 40: 677–681.
41. Aronica, M. A., A. L. Mora, D. B. Mitchell, P. W. Finn, J. E. Johnson, J. R. Sheller, and M. R. Boothby. 1999. Preferential role for NF-kappa B/Rel signaling in the type 1 but not type 2 T cell-dependent immune response in vivo. *J. Immunol.* 163: 5116–5124.
42. Tumang, J. R., A. Owyang, S. Andjelic, Z. Jin, R. R. Hardy, M. L. Liou, and H. C. Liou. 1998. c-Rel is essential for B lymphocyte survival and cell cycle progression. *Eur. J. Immunol.* 28: 4299–4312.
43. Chen, G., K. Hardy, K. Bunting, S. Daley, L. Ma, and M. F. Shannon. 2010. Regulation of the IL-21 gene by the NF-κB transcription factor c-Rel. *J. Immunol.* 185: 2350–2359.
44. Mc Guire, C., L. Elton, P. Wieghofer, J. Staal, S. Voet, A. Demeyer, D. Nagel, D. Krappmann, M. Prinz, R. Beyaert, and G. van Loo. 2014. Pharmacological inhibition of MALT1 protease activity protects mice in a mouse model of multiple sclerosis. *J. Neuroinflammation* 11: 124.
45. Jabara, H. H., T. Ohsumi, J. Chou, M. J. Massaad, H. Benson, A. Megarbane, E. Chouery, R. Mikhael, O. Gorka, A. Gewies, et al. 2013. A homozygous mucosa-associated lymphoid tissue 1 (MALT1) mutation in a family with combined immunodeficiency. *J. Allergy Clin. Immunol.* 132: 151–158.
46. Chinen, J., L. D. Notarangelo, and W. T. Shearer. 2014. Advances in basic and clinical immunology in 2013. *J. Allergy Clin. Immunol.* 133: 967–976.
47. McKinnon, M. L., J. Rozmus, S. Y. Fung, A. F. Hirschfeld, K. L. Del Bel, L. Thomas, N. Marr, S. D. Martin, A. K. Marwaha, J. J. Priatel, et al. 2014. Combined immunodeficiency associated with homozygous MALT1 mutations. *J. Allergy Clin. Immunol.* 133: 1458–1462, e1–e7.
48. Jaworski, M., B. J. Marsland, J. Gehrig, W. Held, S. Favre, S. A. Luther, M. Perroud, D. Golshayan, O. Gaide, and M. Thome. 2014. Malt1 protease inactivation efficiently dampens immune responses but causes spontaneous autoimmunity. *EMBO J.* 33: 2765–2781.
49. Gewies, A., O. Gorka, H. Bergmann, K. Pechloff, F. Petermann, K. M. Jeltsch, M. Rudelius, M. Kriegsmann, W. Weichert, M. Horsch, et al. 2014. Uncoupling Malt1 threshold function from paracaspase activity results in destructive autoimmune inflammation. *Cell Reports* 9: 1292–1305.